Laboratory Experiments on CO_2 Gas Exchange with Wave Breaking

SHUO LI,[a] ALEXANDER V. BABANIN,[a,b] FANGLI QIAO,[b,c] DEJUN DAI,[c] SHUMIN JIANG,[c] AND CHANGLONG GUAN[d]

[a] *Department of Infrastructure Engineering, University of Melbourne, Melbourne, Victoria, Australia*
[b] *Laboratory for Regional Oceanography and Numerical Modeling, National Laboratory for Marine Science and Technology, Qingdao, China*
[c] *First Institute of Oceanography, Ministry of Natural Resources, Qingdao, China*
[d] *College of Oceanic and Atmospheric Sciences, Ocean University of China, Qingdao, China*

(Manuscript received 1 November 2020, in final form 8 July 2021)

ABSTRACT: The CO_2 gas transfer velocity (K_{CO_2}) at air–sea interface is usually parameterized with the wind speed, but to a great extent it is defined by waves and wave breaking. To investigate the direct relationship between K_{CO_2} and waves, laboratory experiments are conducted in a wind-wave flume. Three types of waves are forced in the flume: modulational wave trains generated by a wave maker, wind waves with 10-m wind speed ranging from 4.5 to 15.5 m s^{-1}, and (mechanically generated) modulational wave trains coupled with superimposed wind force. The wave height and wave orbital velocity are found to be well correlated with K_{CO_2} whereas wind speed alone cannot adequately describe K_{CO_2}. To reconcile the measurements, nondimensional equations are established in which gas transfer velocity is expressed as a main function of wave parameters and an additional secondary factor to account for influence of the wind.

KEYWORDS: Wave breaking; Air-sea interaction; Carbon dioxide

1. Introduction

Atmospheric carbon dioxide (CO_2) has been accumulating in the past few decades due to excessive anthropogenic activities including fossil fuel combustion and land use, which exerts impact on global climate change and carbon cycle IPCC (2014). Significant efforts have been made to evaluate the redistribution of CO_2 emissions among global atmosphere, ocean and land (Takahashi et al. 2009; Ballantyne et al. 2012; Wanninkhof et al. 2013; Landschützer et al. 2016; Friedlingstein et al. 2019; DeVries et al. 2019; Delire et al. 2019). The ocean is one of the largest reservoirs to mitigate the increment of atmospheric CO_2, absorbing about 30% of the released CO_2 through gas exchange across the air–sea interface. The CO_2 gas flux F between the atmosphere and ocean is generally described as the product of gas transfer velocity (K_{CO_2}), gas solubility s in seawater, and thermodynamic driving force in terms of the partial pressure difference:

$$F = K_{CO_2} s(pCO_{2w} - pCO_{2a}), \tag{1}$$

where pCO_{2w} and pCO_{2a} denote the water-side and air-side CO_2 partial pressure, respectively. Oceans may act as source ($pCO_{2w} > pCO_{2a}$) or sink ($pCO_{2w} < pCO_{2a}$) zones for the atmospheric CO_2 with varied net gas fluxes (Takahashi et al. 2009). Scientific interest also lies in the decadal variability of air–sea CO_2 fluxes, with evidence indicating that the ocean is experiencing an increasing rate of CO_2 uptake in recent decades (Ishidoya et al. 2012; Landschützer et al. 2014; Landschützer et al. 2016; Friedlingstein et al. 2019). However, accurate estimation of air–sea CO_2 gas fluxes is still challenging because of the large uncertainties derived from the spatially and temporally sparse measurements of CO_2 partial pressure pCO_2, gaps among parameterizations for gas transfer velocity (K_{CO_2}) and the uncertainties of the dynamic variables (e.g., wind force) in K_{CO_2} parameterizations IPCC (2014). With more ocean pCO_2 data being collected from field observations, such as the Surface Ocean CO_2 Atlas (SOCAT) (Bakker et al. 2016) and Global Surface pCO_2 (LDEO) Database (Takahashi et al. 2019), methods to reconstruct the global distribution of pCO_2 with restrained errors have been developed (Rödenbeck et al. 2013; Landschützer et al. 2014; Jones et al. 2015; Denvil-Sommer et al. 2019). K_{CO_2} in Eq. (1) is a kinetic function of environmental forcing factors such as wind speed, wave properties (e.g., height and steepness) and bubble production (size and amount—both related to the wave breaking). Because K_{CO_2} is critical to the prediction of CO_2 fluxes in the climate change context, its parameterization has been a major research topic for years.

Considering that most of the relevant dynamic processes at air–sea interface can scale with the wind, K_{CO_2} is generally parameterized with the wind speed through a linear (Jähne et al. 1979; Liss and Merlivat 1986), quadratic (Wanninkhof 1992; Nightingale et al. 2000; Ho et al. 2006; Sweeney et al. 2007) or cubic relationship (McGillis et al. 2004; Edson et al. 2011). Nonetheless, gaps among wind-based equations still exist especially for the circumstances of developed wind–sea states, implying that the wind speed alone may not be sufficient to quantify K_{CO_2}. Since CO_2 is sparingly soluble gas, K_{CO_2} is regulated by water-side turbulence (Jähne et al. 1987) that is frequently produced by wave orbital motion and wave breaking (Babanin 2006; Gemmrich 2010; Sutherland and Melville 2015; Lee et al. 2017) in addition to the wind. The breaking waves also produce bubble clouds that significantly facilitate the gas fluxes because of extended air–water interface area and enhanced turbulence when bubbles rise up (Asher et al. 1996; Wanninkhof et al. 2009). The importance of wave breaking on air–sea interaction has also been discussed in Melville (1996)

Corresponding author: Shuo Li, shuo.lee518@gmail.com

DOI: 10.1175/JPO-D-20-0272.1

© 2021 American Meteorological Society. For information regarding reuse of this content and general copyright information, consult the AMS Copyright Policy (www.ametsoc.org/PUBSReuseLicenses).
Brought to you by IFREMER/BILIOTHEQUE LA | Unauthenticated | Downloaded 10/10/22 09:59 AM UTC

and Babanin (2011). Because of the lost energy, wave breaking enhances intensity of the near-surface turbulence by up to three orders of magnitude, and it produces bubbles and may spend up to 50% of energy loss on work against the buoyancy force acting on these bubbles. Wave growth and ultimately its breaking are connected with the wind, hence there is a correlation between CO_2 gas transfer and wind speed, but this is by far not a direct connection because the breaking is caused by nonlinear evolution of waves (or wave superposition), not the wind (Tulin and Waseda 1999; Babanin et al. 2011). Therefore, physical models for K_{CO_2} that include wave effect explicitly could provide improved flux estimates over limited spatial and temporal scales that depart from the mean behavior of the wind-based formulas and also offer a way to extend gas transfer estimates to conditions beyond the validity of the wind-based formulas (e.g., tropical cyclones).

Research on the wave-affected gas transfer shows that the mean square slope of the waves is an appropriate index for the gas transfer rate (Jähne et al. 1987; Frew et al. 2004). In addition, the dependence of gas transfer rate on Schmidt number Sc, which is the ratio of fluid kinematic viscosity and mass diffusivity, changes from $Sc^{-2/3}$ to $Sc^{-1/2}$ because of the wavy surface. Zappa et al. (2001, 2004) employed infrared technique to detect the microwave breaking under low to moderate wind speeds in the wave tank and found that the gas transfer velocity could be scaled with fractional area coverage of microbreakers. Similarly, the whitecap coverage at open ocean is also utilized to scale the gas transfer rate (Zhao et al. 2003; Woolf 2005). Zhao and Toba (2001) demonstrated that a variable named wind–sea Reynolds number is superior to the wind speed in describing whitecap coverage. Thus, the wind–sea Reynolds number is also proposed for the study of gas transfer (Toba et al. 2006) and could be written as

$$R_H = \frac{u_* H_s}{\nu_a} \quad \text{and} \quad R_B = \frac{u_*^2}{\omega_p \nu_a}, \tag{2}$$

where R_H and R_B represent two forms of the Reynolds number, u_* is the wind friction velocity, H_s is the significant wave height, ν_a is air kinematic viscosity, and ω_p is the peak angular velocity of wave spectrum. The hybrid parameters R_H and R_B that contain both wind speed and wave parameters are interpreted as a measure of the turbulence intensity generated by wind waves and employed to explain the diversity of previous wind-based parameterizations of gas transfer through emphasizing the role of sea state (Zhao et al. 2003; Woolf 2005). Brumer et al. (2017) adopted the similar Reynolds number by replacing ν_a in R_H and R_B with water viscosity ν_w and reconciled four datasets from open ocean with reduced uncertainties. Other than turbulence, the breaking waves may induce bubble clouds as well. The bubble-mediated gas transfer is observed to be evident especially for the low-solubility gases at high wind speeds (Woolf et al. 2007; Bell et al. 2017; Krall et al. 2019). To date, accurate modeling of the behavior of bubbles remains an active research subject and the bubble-mediated gas transfer is commonly scaled with the wind speed (Stanley et al. 2009; Liang et al. 2013).

Laboratory experiment is a practical approach to investigate the gas transfer with the advantage that the environmental forces such as wind and waves can be properly controlled and quantified. Ocampo-Torres et al. (1994) reported the gas transfer in a wind-wave flume where the tank water was saturated with CO_2 and the wind waves were generated with the 10-m wind speed ranging from 1 to 24 m s^{-1}. The gas transfer velocity was obtained by monitoring CO_2 concentration change in the water and air. Based on the similar framework, Iwano et al. (2013) extended the wind speed up to 70 m s^{-1} in the laboratory. A substantial enhancement of the gas flux was observed when the wind speed exceeded 33 m s^{-1} and induced intensive wave breaking. Despite the agreement on the critical role of wave breaking on the gas transfer, the exact nature of their relationship remains elusive. The present work aims to correlate gas transfer velocity with the characteristics of waves in the laboratory. To examine the specific effect of breaking waves without wind force, we first simulate the ocean wave breaking ascribed to nonlinear evolution by exerting modulational perturbations to the laboratory deep-water waves that are generated by mechanical wave maker (Benjamin and Feir 1967; Tulin and Waseda 1999; Babanin et al. 2010). The more complicated circumstances are also created, where the breaking waves with diverse wave ages are coupled with superimposed wind.

2. The experiments

The facility used for experiments is a wind-wave flume (Fig. 1) that is 45 m long, 1.8 m high, and 1 m wide available at the First Institute of Oceanography in China. The tank is filled with freshwater up to 1.2 m. The wind fan is installed above the wave tank with air channel for wind-forced waves. A mechanical wave maker is located upstream. It is programmable and able to generate regular waves, steep enough to lead to wave breaking. At the downstream end of wave tank, a beach is designed for damping wave energy (more than 95%) to prevent the reflection of waves.

Various sensors were deployed along the wave tank to measure physical and chemical variables. Water surface elevation was monitored by four resistance-type wave gauges at 50-Hz sampling rate. They were individually located at the distance of 6.2, 14.0, 16.6, and 18.0 m from the wave maker. A vertical array of five pitot tubes (5-cm spaced) was installed at the position of 10 cm before wave gauge 3, and the lowest tube was 15 cm above flat water surface. The wind speed was recorded at 10 Hz by a computer that was connected to the pitot tubes. An acoustic Doppler velocimeter (ADV) was collocated with wave gauge 3 to assess particle motions in the water, although the data are not used in the present work. Located at 50 cm downstream of wave gauge 3, the tubes for taking air and water samples were installed in the flume, and further connected to the CO_2 analysis devices. Two thermometers were placed at the rear of wave tank for the temperature of air and water, respectively. Air conditioners in the laboratory were always running during the experiments so that the temperatures at different locations of wave tank were almost the same. Outside the wave tank, a Canon digital camera

Brought to you by IFREMER/BILIOTHEQUE LA | Unauthenticated | Downloaded 10/10/22 09:59 AM UTC

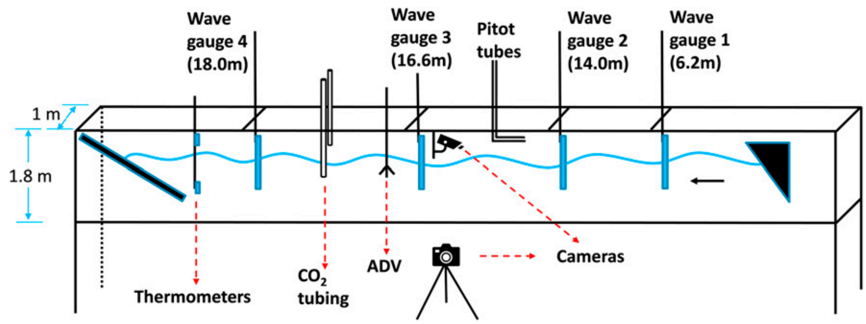

FIG. 1. Schematic showing the deployment of probes in the wave tank. There were four resistance-type wave gauges at 6.2, 14.0, 16.6, and 18.0 m from the wave maker on the right. Close to wave gauge 3, a set of pitot tubes, ADV, and sampling tubes for CO_2 analysis were installed. Outside the wave tank, a Canon camera and a video camera were used to record waves. At the rear of the wave tank, a pole attached with two thermometers was placed for the measurement of air and water temperature.

and a video camera were employed to observe wave-breaking processes. In addition, the ambient air pressure in the laboratory was recorded in the experiments. The instrument for CO_2 analysis was the Apollo pCO_2 system (model AS-P2 by Apollo SciTech), which incorporated a shower-head air–water equilibrator, a multiposition valve, and a CO_2 analyzer (CRDS model G2301 by Picarro) with high precision (<0.15 and <0.05 ppm for 5-s and 5-min measurements, respectively). The tank water was delivered into the equilibrator with a flow rate of 2.5 L min^{-1} to contact the airstream. After reaching equilibrium, the water was returned to the rear of tank and the equilibrated gas was analyzed as the water-side CO_2 concentration. The multiposition valve in the pCO$_2$ system was switched between the measurement of equilibrated gas samples and air samples from the flume. A drying section was also assembled to remove water vapor from the gas stream. Standard gases with CO_2 concentration of 400.0, 600.7, 799.2, and 1000.6 ppm were used to calibrate the CO_2 analyzer.

The purpose of our experiment was to evaluate the CO_2 transfer rate in terms of different wave conditions. As listed in Table 1, the experimental cases were divided into three categories according to the initial wave input. In cases A1–A10, deep-water wave trains seeded with sideband were generated by mechanical wave maker without wind force. The wave groups were unstable in the propagation due to modulational instability, and the initial wave input parameters were chosen (Babanin et al. 2007) so that the breaking onset was around the location of wave gauge 2. The waves of randomly selected three cases (A5, A9, and A10) were then used to couple with different superimposed wind in B1–B6. The purpose was to observe the wave breaking modified by wind force and the resulted gas transfer rate. The wind was blowing in the same direction with the mechanically generated waves. In C1–C6, the waves were forced only by wind with 10-m wind speed U_{10} ranging from 4.5 to 15.5 m s^{-1}. The mechanically generated wave signal in A1–A10 and B1–B6 was the combination of a carrier sinusoidal wave and one resonant sideband. The properties of carrier wave including the frequency f_0, amplitude a_0, and steepness ε_0 ($=a_0k_0$, where k_0 is the wavenumber) are listed in Table 1. The frequency of the sideband f_+ was close to f_0, whereas the amplitude of the sideband a_+ was much smaller than a_0. The Benjamin–Feir index BFI [$=\varepsilon_0/(\Delta k/k_0)$], where Δk is the wavenumber difference between carrier wave and sideband) was used to represent the instability of wave trains.

The probes of wind and waves were running simultaneously with the pCO_2 system in the experiment. For cases A1–A10 and B1–B6, which contain the mechanically generated waves, the wave records are processed with the same method. Taking case A1 for example, the surface elevation measured by wave gauge 1 to 4 is shown in Fig. 2. The wave groups were clearly modulated by reaching wave gauge 2. The steep waves eventually broke around wave gauge 3 and 4, which was recorded by cameras. By shifting the time frame of wave records, the breaking events that are usually accompanied with evident wave height drop or deformation of wave shape can be identified by examining breaking pattern in videos taken onsite. The breaking pattern refers to the periodic breaking events due to the modulation of same initial wave packets in one case. The records of wave gauge 2 and 4 are shifted relative to that of gauge 3 for a period $t = \Delta X/C'_p$, where ΔX is the fixed distances between wave gauges (i.e., 2.6 m for wave gauge 2–3 and 1.4 m for gauge 3–4), C'_p is the phase speed of waves. It is noted that C'_p is estimated through linear wave theory for sampled non-breaking waves at wave gauge 3. Thus C'_p is an approximation to the varied wave phase speeds. Figure 3 shows the well-matched wave records and the recognized breakers with marks on their crests. The two waves that are marked with squares at wave gauge 2 (blue dashed line) became steep and broke before reaching wave gauge 3 (red line). Similarly, the wave marked with star was breaking at gauge 3. It should be stressed that the recognized breaking events must coincide with the observed breaking pattern in videos. The breakers that are upstream close to the CO_2 sampling spot are employed to correlate with gas transfer rate. For the young wind waves in cases C1–C6, the breakers are selected by using the criterion for ultimate steepness (≤ 0.44) of individual waves that are subject to modulational instability (Babanin et al. 2007, 2010). The surface wave parameters are listed in Table 1: H_b denotes

Brought to you by IFREMER/BIBLIOTHEQUE LA | Unauthenticated | Downloaded 10/10/22 09:59 AM UTC

TABLE 1. Experimental parameters of all cases: f_0, a_0, and ε_0 are wave frequency, amplitude, and steepness of carrier sinusoidal waves, respectively; f_+ and a_+ are sideband frequency and amplitude, respectively; BFI is Benjamin–Feir index; U_{10} is 10-m wind speed; H_b, U_{wb}, and b_T are breaker's mean wave height, mean wave orbital velocity, and breaking probability at wave gauge 3, respectively; U_{wm}, H_s, ε, C_p/U_{10}, and T_z are mean wave orbital velocity, significant wave height, mean wave steepness, wave age, and mean upcrossing wave period at wave gauge 3, respectively; K_{600} is gas transfer velocity in 20°C freshwater.

Case No.	f_0 (Hz)	a_0 (m)	ε_0	f_+ (Hz)	a_+ (m)	BFI	U_{10} (m s^{-1})	H_b (m)	U_{wb} (m s^{-1})	b_T	U_{wm} (m s^{-1})	H_s (m)	ε	C_p/U_{10}	T_z (s)	K_{600} (10^{-6} m s^{-1})
A1	1.2	0.035	0.20	1.32	0.010	0.95	—	0.15	0.60	0.092	0.32	0.13	0.24	—	0.84	1.077
A2	1.2	0.052	0.30	1.33	0.006	1.36	—	0.18	0.70	0.103	0.48	0.19	0.36	—	0.85	1.404
A3	1.0	0.050	0.20	1.10	0.024	0.95	—	0.25	0.82	0.073	0.40	0.19	0.25	—	1.00	1.350
A4	1.3	0.029	0.20	1.43	0.007	0.95	—	0.10	0.36	0.101	0.30	0.12	0.23	—	0.83	0.773
A5	1.1	0.041	0.20	1.21	0.014	0.95	—	0.23	0.81	0.090	0.35	0.16	0.24	—	0.92	1.519
A6	0.9	0.061	0.20	1.04	0.035	0.60	—	0.30	0.90	0.069	0.43	0.22	0.25	—	1.11	1.751
A7	1.1	0.033	0.16	1.24	0.019	0.59	—	0.15	0.53	0.111	0.31	0.14	0.22	—	0.91	1.257
A8	1.1	0.051	0.25	1.24	0.014	0.94	—	0.20	0.72	0.111	0.42	0.19	0.29	—	0.91	1.450
A9	1.0	0.055	0.22	1.11	0.023	0.95	—	0.24	0.76	0.098	0.42	0.20	0.28	—	1.00	1.737
A10	0.9	0.055	0.18	1.02	0.039	0.61	—	0.29	0.87	0.120	0.40	0.21	0.23	—	1.11	3.009
B1	0.9	0.055	0.18	1.02	0.039	—	11.21	0.29	0.85	0.121	0.46	0.24	0.26	0.158	1.11	4.931
B2	0.9	0.055	0.18	1.02	0.039	—	6.77	0.28	0.82	0.122	0.42	0.22	0.24	0.260	1.11	1.956
B3	1.1	0.041	0.20	1.21	0.014	—	9.14	0.20	0.74	0.087	0.40	0.18	0.28	0.157	0.90	3.110
B4	1.1	0.041	0.20	1.21	0.014	—	13.43	0.24	0.88	0.086	0.52	0.22	0.36	0.109	0.90	4.210
B5	1.0	0.055	0.22	1.11	0.023	—	8.85	0.26	0.86	0.098	0.46	0.22	0.29	0.181	1.00	3.933
B6	1.0	0.055	0.22	1.11	0.023	—	13.43	0.27	0.88	0.096	0.55	0.25	0.35	0.119	0.99	7.159
C1	—	—	—	—	—	—	4.46	0.02	0.21	0.239	0.15	0.02	0.38	0.091	0.25	0.093
C2	—	—	—	—	—	—	6.88	0.03	0.29	0.371	0.22	0.04	0.40	0.080	0.34	0.285
C3	—	—	—	—	—	—	9.19	0.04	0.34	0.488	0.27	0.05	0.45	0.067	0.38	0.701
C4	—	—	—	—	—	—	11.12	0.05	0.38	0.559	0.31	0.07	0.47	0.061	0.41	1.027
C5	—	—	—	—	—	—	13.25	0.07	0.44	0.665	0.39	0.09	0.52	0.057	0.45	—
C6	—	—	—	—	—	—	15.44	0.09	0.51	0.732	0.45	0.12	0.56	0.053	0.49	2.848

the mean wave height of breakers before breaking; U_{wb} is the mean orbital velocity of breakers and is estimated as $\overline{a\omega}$, where a is the breaker's amplitude, ω is the wave radian frequency and is computed based on the dispersion relation of deep water waves in linear wave theory, and the overbar denotes the mean of the quantity beneath it; b_T is the breaking probability, which is defined as the percentage of breaking crests within the sequence of all wave crests. The features of all waves at the location of wave gauge 3 are also presented; H_s is the significant wave height; U_{wm} is the mean orbital velocity and is calculated using the same method as for U_{wb}; ε is the mean wave steepness and equal to $\overline{ak}$, where a and k are wave amplitude and wavenumber, respectively; T_z is the mean upcrossing wave period; C_p/U_{10} denotes the mean wave age, where C_p is the phase speed of waves and U_{10} is the 10-m wind speed. The drag coefficient c_d is computed to be 0.0013 in case C6 with a clear logarithmic wind profile. Because a wind-dependent c_d has slight influence on the coefficients of our final parameterizations, constant c_d (=0.0013) is used here to compute U_{10} and friction velocity. In addition, with propagating waves in cases A1–A6, there should be disturbance in the air. However, the resulting turbulent velocity of air cannot be accurately estimated and its impact on gas transfer is ignored.

Before the start of each experiment, the tank water was dissolved with excessive amount of CO_2 gas and fully mixed by water pumps to create air–water CO_2 partial pressure difference. Meanwhile, the wind channel was open to let the laboratory air in and maintain a low level of air-side CO_2 concentration in the flume. By the start of experiment, the CO_2 concentration detected by the analyzer in air and water were around 450 and 950 ppm, respectively. The measurements of CO_2 for two cases (A6 and A7) are shown in Fig. 4. The time length for each case was about 2 h. The upper and lower envelope within each case are the CO_2 concentration of

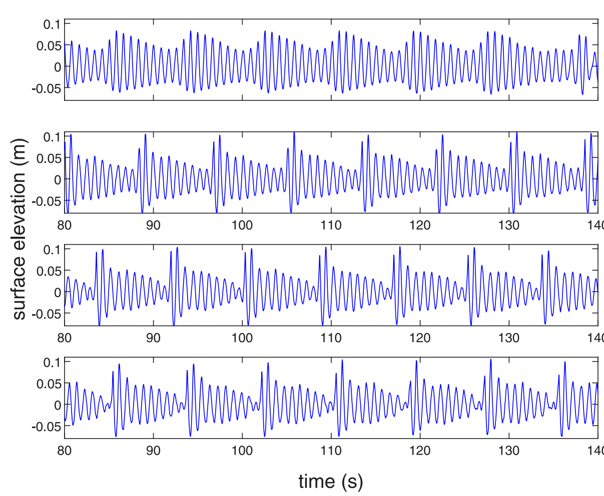

FIG. 2. Surface elevation measured by wave gauge (top)1, (top middle) 2, (bottom middle) 3, and (bottom) 4 in case A1. The wave groups were clearly modulated during the propagation, especially from wave gauge 1 to gauge 2.

Brought to you by IFREMER/BILIOTHEQUE LA | Unauthenticated | Downloaded 10/10/22 09:59 AM UTC

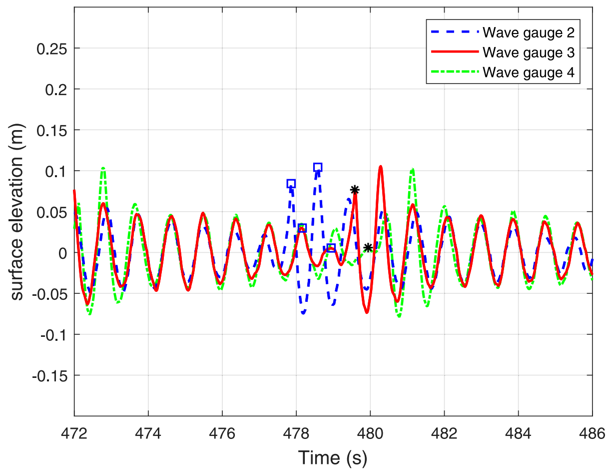

FIG. 3. Breakers that are identified by shifting the time frame of wave records in case A1. The two waves that are marked with squares at wave gauge 2 (blue dashed line) became steep and broke by reaching wave gauge 3 (red line). Similarly, the wave marked with star is a breaker captured between wave gauge 3 and 4. The features of waves around wave gauge 3, which is near to the CO_2 sampling spot, are used to correlate with CO_2 gas transfer rate.

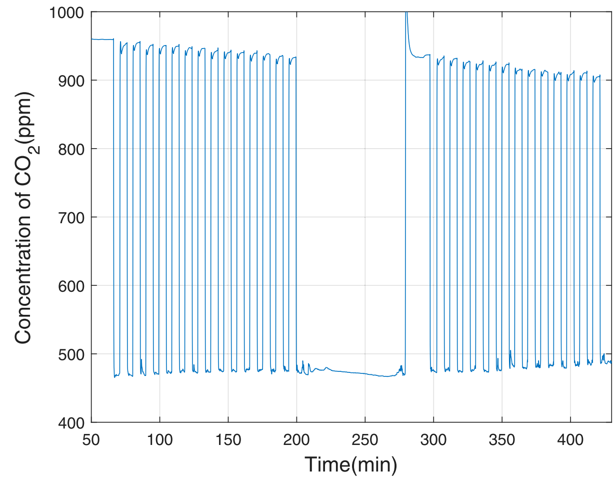

FIG. 4. The measurements of CO_2 concentration for two cases (A6 and A7). The time length for each case was about 2 h. The upper and lower envelope are the CO_2 concentration of equilibrated gas and air, respectively. The concentration of CO_2 in water (upper envelope) is always decreasing during experiments.

equilibrated gas (C_g) and air (C_a), respectively. Following Ocampo-Torres et al. (1994), the gas transfer rate K_{CO_2} can be estimated as

$$\frac{\partial C_g}{\partial t}\frac{V_w}{A} = -K_{CO_2}(C_g - C_a), \tag{3}$$

where V_w and A is the water volume and surface area that are involved with the gas exchange processes. So V_w/A represents the height of water column, which is related to the depth of turbulent mixing layer. Thomson et al. (2016) suggested that the turbulence could be transported down to wave trough due to orbital motion, so in our work the depth of upper mixing layer is scaled with the wave height of breakers H_b. The calculated K_{CO_2} is further corrected to 20°C of freshwater with Schmidt number Sc_{600} (=600), which can be written as

$$\frac{K_{CO_2}}{K_{600}} = \left(\frac{Sc_{CO_2}}{Sc_{600}}\right)^{-0.5}, \tag{4}$$

where K_{600} represents the corrected transfer velocity (see Table 1) and Sc_{CO_2} is the Schmidt number of water in the flume. The power of Sc is empirically determined as −0.5 for wavy surfaces (Jähne et al. 1987).

3. New parameterization for CO_2 gas transfer velocity

Each group of the experiments is separately studied first by showing relatively high correlations between the gas transfer velocity K_{600} and wind/wave parameters in Fig. 5. It is worth noting that other wind/wave parameters not shown in Fig. 5 may also correlate with K_{600} (see Fig. 6).

In cases A1–A10, mechanically generated waves promote the gas transfer. K_{600} is found correlated with breaker's mean wave height H_b and orbital velocity U_{wb} in Figs. 5b and 5d, but the correlation coefficients are much improved after multiplying H_b or U_{wb} by breaking probability b_T in Figs. 5c and 5e although the dependence of K_{600} on b_T is very weak (Fig. 5). It can be interpreted that b_T determines the frequency of water mixing events due to wave breaking, while larger wave height and orbital motion imply more turbulence in these events. In Fig. 5f, K_{600} is also well correlated with the rate of energy loss P_b of breaking waves; P_b is defined as

$$P_b = \frac{\sum(H_{b1}^2 - H_{b2}^2)}{\Delta t}, \tag{5}$$

where H_{b1} and H_{b2} are the wave height before and after wave breaking, respectively. They are estimated through the measurements of wave gauge 3 and 4 accordingly. Note that the estimations of H_{b1} and H_{b2} do not precisely represent the wave height of incipient breakers and residual waves after breaking because the position of wave gauges are fixed. Symbol Σ denotes the summation of energy loss of selected breakers at the time length of Δt, which is a constant (1600 s) in our work. Rate P_b contains the information of wave-breaking probability and breaking strength $[=(H_{b1}^2 - H_{b2}^2)/H_{b1}^2]$. The energy loss of breakers is passed to the turbulence whose production rate may be represented by $b_T H_b$ or $b_T U_{wb}$. Additionally, the computed correlation between P_b and $b_T H_b$ is as high as 96%. The preliminary results of A1–A10 demonstrate that wave breaking can still enhance CO_2 gas fluxes without wind force and that wave properties are directly relevant to the CO_2 transfer rate.

In cases B1–B6 where mechanically generated waves are coupled with superimposed wind, K_{600} shows good correlation with significant wave height H_s, mean wave orbital velocity U_{wm}, 10-m wind speed U_{10}, and wave age C_p/U_{10} in Figs. 5g–j, respectively. The breaking-wave parameters (b_T, H_b, and U_{wb})

Brought to you by IFREMER/BILIOTHEQUE LA | Unauthenticated | Downloaded 10/10/22 09:59 AM UTC

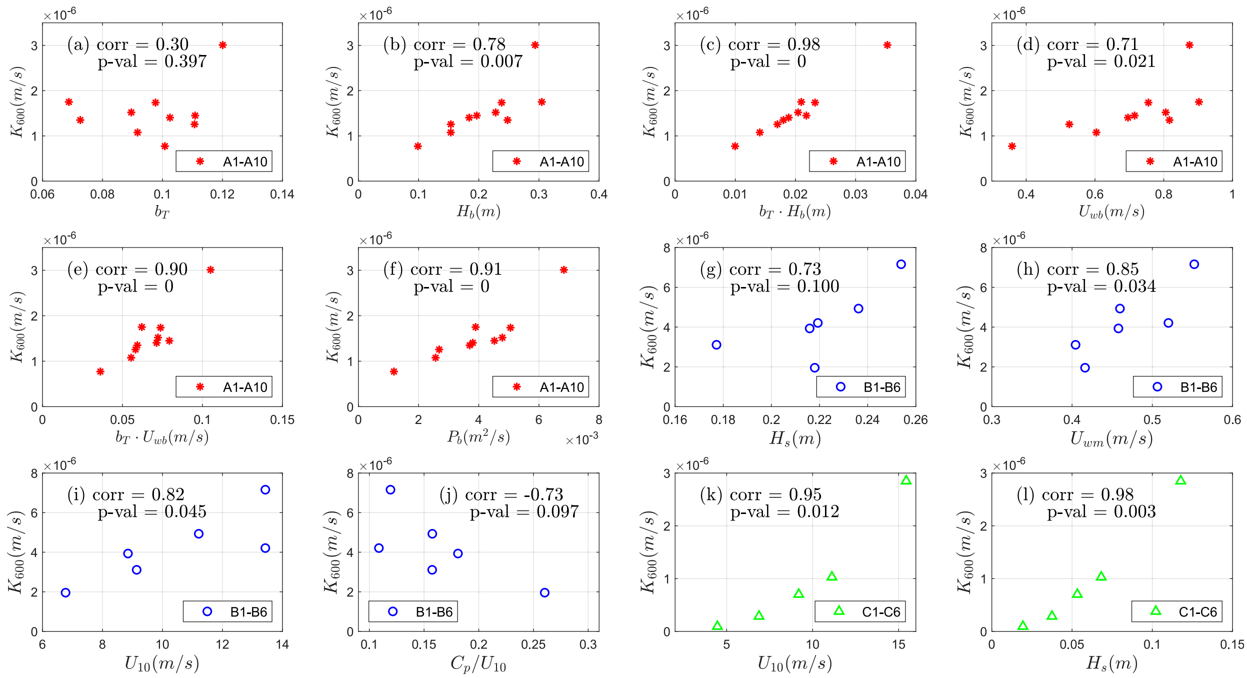

FIG. 5. The Pearson's correlation coefficient and p value between CO_2 gas transfer velocity K_{600} and parameters of the wind and waves: shown is K_{600} in cases A1–A10 vs (a) wave-breaking probability b_T, (b) mean wave height of breakers H_b, (c) product of breaking probability and mean wave height of breakers $b_T H_b$, (d) mean wave orbital velocity of breakers U_{wb}, (e) product of breaking probability and mean wave orbital velocity of breakers $b_T U_{wb}$, (f) mean energy loss of breakers upstream nearest the CO_2 sampling tubes per unit of time P_b; K_{600} in cases B1–B6 vs (g) significant wave height H_s, (h) mean wave orbital velocity U_{wm}, (i) 10-m wind speed U_{10}, (j) wave age C_p/U_{10}; and K_{600} in cases C1–C6 vs (k) 10-m wind speed U_{10} and (l) significant wave height H_s.

do not perform well in these occasions. As compared with cases A5, A9, and A10, the wind force influences the modulation process of unstable waves and changes the features of wave breaking. The complex effects of wind on modulational waves with respect to wave spectra, breaking probability and breaking strength have been discussed in previous studies (Waseda and Tulin 1999; Babanin et al. 2010; Galchenko et al. 2012). The wind also ripples the smooth surface of nonbreaking mechanically generated waves, which implies that energy transfers from wind to these waves thus creating more turbulence in water and enhancing gas transfer. This conforms with the results that mean wave age is inversely proportional to the gas transfer rate (Fig. 5j), since the inverse of wave age could be a measure of the energy shift efficiency from wind to waves. It may also be the reason why statistical parameters H_s and U_{wm}, which are estimated based on all waves, rather than breaking-wave parameters (H_b or U_{wb}), are in good correlation with K_{600}. Therefore, the nonbreaking waves should be important too, although their contribution in comparison with that of breaking waves to gas transfer needs further study.

In cases C1–C6, the young wind waves at fixed fetch grow with the strengthened wind force. K_{600} correlates very well with 10-m wind speed and significant wave height in Figs. 5k and 5l. Similarly, other wave parameters such as wave orbital velocity and breaking probability also scale well with K_{600}, which implies that the appropriate parameter cannot be determined through these cases alone.

The gas transfer velocity in terms of wind/wave parameters for all experiments is shown in Fig. 6. For wave-breaking probability b_T (Fig. 6a), wave steepness ε (Fig. 6b), and mean wave period T_z (Fig. 6c), there is positive correlation within each group of experiments but these parameters cannot reconcile the results of three groups (groups A, B, and C). On the other hand, wave height and orbital velocity work well in improving the correlations in Figs. 6d–g. The significant wave height H_s and mean wave orbital velocity U_{wm} in Figs. 6f and 6g are better correlated with K_{600}, when compared with the distribution in Figs. 6d and 6e for breaker's wave height H_b and orbital velocity U_{wb}. The correlation of K_{600} and U_{10} in Fig. 6h seems acceptable, but the results of two experimental groups (B1–B6 and C1–C6) are clearly distinguishable because wind field is coupled with different wave states. It may also account for the discrepancies of previous wind-based parameterizations that are statistically fitted from different observational datasets. This issue is more evident for the wave age C_p/U_{10} in Fig. 6i, which leads to a low correlation coefficient. Besides, U_{10} and C_p/U_{10} are unsuitable for cases A1–A10 where the wave breaking dominates gas transfer without wind.

Although individual wave parameters are assessed in Fig. 6, these parameters may also be interrelated, such as H_s and U_{wm} in Fig. 7a. Additionally, a combination of some parameters may scale well with K_{600} too. For example, $T_z^3\varepsilon^3$, which is proportional to U_{wm}^3, is in a good correlation with K_{600} in Fig. 7b.

Brought to you by IFREMER/BIBLIOTHEQUE LA | Unauthenticated | Downloaded 10/10/22 09:59 AM UTC

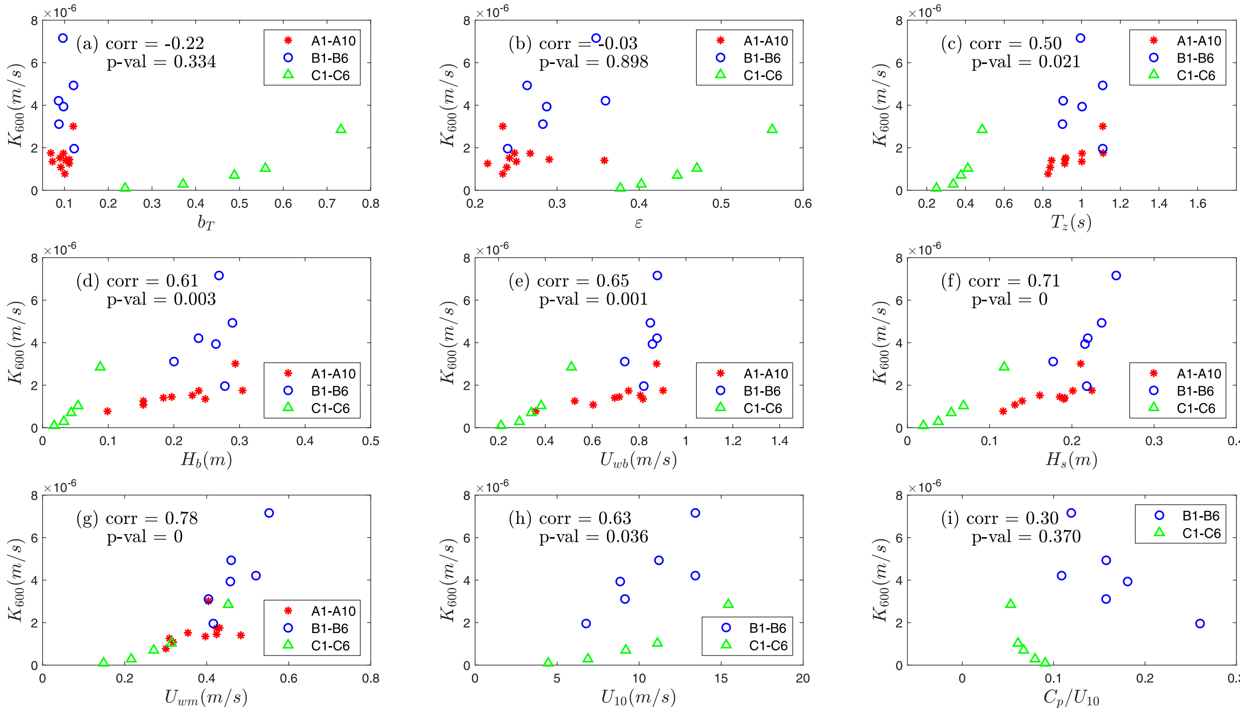

FIG. 6. The Pearson's correlation coefficient and p value between K_{600} and wind/wave parameters in all cases: shown is K_{600} vs (a) b_T, (b) wave steepness ε, (c) mean wave period T_z, (d) H_b, (e) U_{wb}, (f) H_s, (g) U_{wm}, (h) U_{10}, (i) and C_p/U_{10}.

By analyzing the gas fluxes under environmental forces, water-side turbulence generated by breaking waves and wind energy input (to both breakers and nonbreaking waves) determine the gas transfer velocity. In view of the direct dependence of turbulence on waves and the high correlation of wave parameters with K_{600}, the wave height and orbital velocity seem more suitable than wind speed for the parameterization of gas transfer. Therefore, similar wind–sea Reynolds numbers as R_H in Eq. (2) are formulated in Eq. (6) to denote the wave-related turbulence. The wind speed component in R_H is replaced with wave orbital velocity as the representative scale of speed. Additionally, the viscosity of water ν_w is employed instead of ν_a:

$$R_{\mathrm{HM}} = \frac{H_s U_{\mathrm{wm}}}{\nu_w} \quad \text{and} \quad R_{\mathrm{HB}} = \frac{H_b U_{\mathrm{wb}}}{\nu_w}. \tag{6}$$

The R_{HM} and R_{HB} have the same structure but comprise different wave parameters: R_{HM} contains H_s and U_{wm}, which are statistically based on all waves, whereas R_{HB} highlights the features of breaking waves (H_b and U_{wb}). Note that H_s is not independent of U_{wm} as demonstrated in Fig. 7a because U_{wm} is equal to $\overline{(H/2)\omega}$, where H is the wave height and ω is the wave radian frequency.

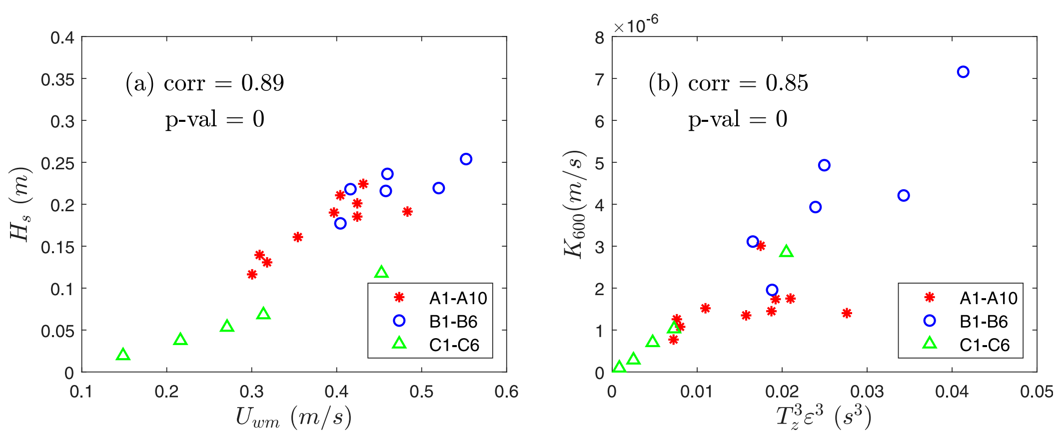

FIG. 7. (a) The correlation between H_s and U_{wm}, and (b) the correlation between K_{600} and $T_z^3\varepsilon^3$.

Brought to you by IFREMER/BILIOTHEQUE LA | Unauthenticated | Downloaded 10/10/22 09:59 AM UTC

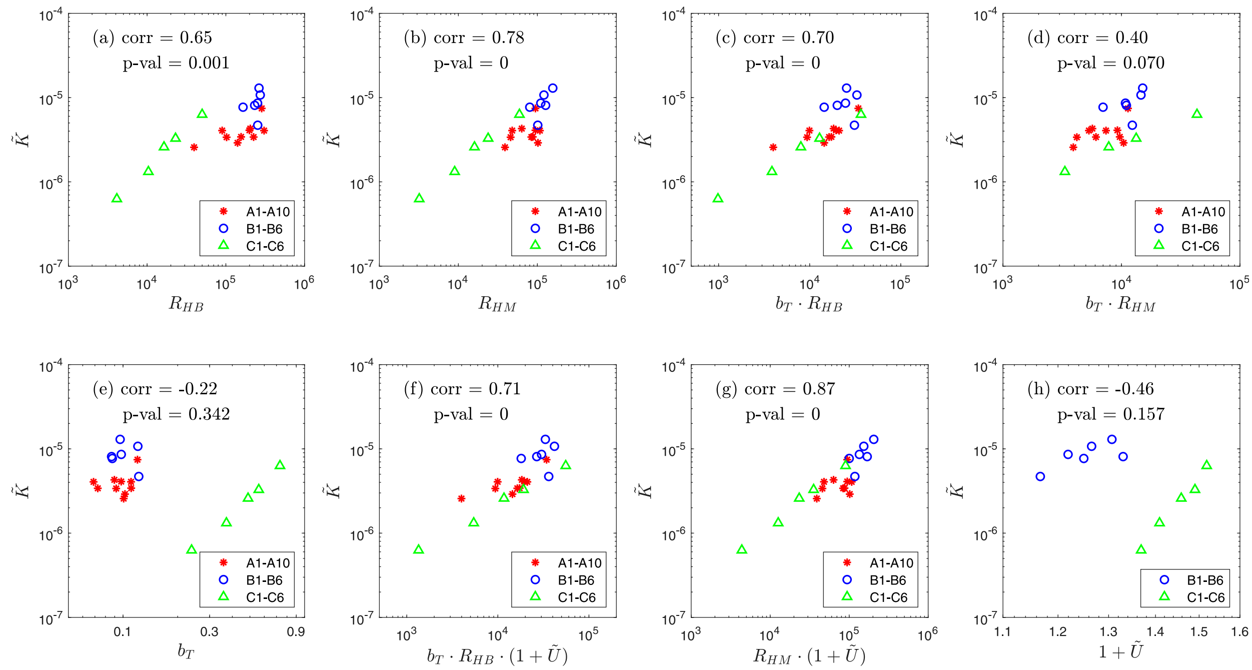

FIG. 8. Nondimensional CO_2 gas transfer velocity $\tilde{K}$ vs (a) Reynolds number $R_{\rm HB}$, (b) Reynolds number $R_{\rm HM}$, (c) $b_T R_{\rm HB}$, (d) $b_T R_{\rm HM}$, (e) b_T, (f) product of b_T, $R_{\rm HB}$ and scaled wind speed, (g) product of $R_{\rm HM}$ and scaled wind speed, and (h) scaled wind speed.

In the study of Toba et al. (2006), a nondimensional gas transfer velocity is defined as K_{600}/U_{10} so that its relationship with R_H can be examined. Here, K_{600} is reasonably scaled with the mean wave orbital velocity $U_{\rm wm}$ instead of U_{10} to avoid the dependence on dimensional parameters and be applicable for experiments A1–A10. The nondimensional gas transfer velocity $\tilde{K}$ is defined as

$$\tilde{K} = K_{600}/U_{\rm wm}. \tag{7}$$

Following Lenain and Melville (2017), the wind speed is also scaled as

$$\tilde{U} = \frac{U_*}{\sqrt{gH_s}}, \tag{8}$$

where $\tilde{U}$ is nondimensional wind speed, U_* is the wind friction velocity, and g is gravitational acceleration. Note that $(gH_s)^{1/2}$ is proportional to wave peak phase velocity C_p in fetch-limited condition. Thus, $\tilde{U}$ is analogous to the inverse of wave age and could denote the efficiency of energy transfer from wind to waves.

The nondimensional parameters are presented in Fig. 8. Parameter $\tilde{K}$ is correlated with $R_{\rm HB}$ and $R_{\rm HM}$ in Figs. 8a and 8b, although the correlation with $R_{\rm HB}$ is relatively weak. It is worth mentioning that the better correlation for $R_{\rm HM}$ is because of the good correlations between K_{600} and H_s, $U_{\rm wm}$ in Figs. 6f and 6g rather than possible self-correlation caused by $U_{\rm wm}$. As discussed earlier, the gas transfer rate for experiments A1–A10 is highly correlated with the product of breaking probability b_T and wave height (or orbital velocity) of the breakers while b_T is not preferred for B1–B6 since the effect of nonbreaking waves need to be considered as well. For parameters $R_{\rm HB}$ and $R_{\rm HM}$, the selection of their components highlights the importance of breaking waves and all waves, respectively. Therefore, we consider multiplying $R_{\rm HB}$ by b_T and the resulted correlation is improved in Fig. 8c. On the contrary, b_T seems to be redundant for $R_{\rm HM}$ in Fig. 8d. We should also mention that b_T alone is not capable of reconciling the results in Fig. 8e. The wind plays an indirect role by transferring energy into waves and a direct but insignificant role by creating turbulence beyond the water surface. So the wind energy transfer efficiency is parameterized as an enhancement factor $(1+\tilde{U})$, which is combined with $b_T R_{\rm HB}$ and $R_{\rm HM}$ in Figs. 8f and 8g. The corresponding correlations are improved and $(1+\tilde{U})$ alone is not well correlated with $\tilde{K}$ in Fig. 8h. The expressions of $b_T R_{\rm HB}(1+\tilde{U})$ and $R_{\rm HM}(1+\tilde{U})$ would converge to the no-wind conditions ($b_T R_{\rm HB}$ and $R_{\rm HM}$) when the wind force approaches zero. It should be emphasized that our parameterization is established based on physical analysis and correlation index. As shown in Fig. 7b, gas transfer velocity could also be scaled with the combination of other wave parameters, but appropriate physical explanation and validation are required.

With the proposed parameterizations, the fit results are shown in Fig. 9. The error bars of $\tilde{K}$ represent the standard error of the mean. The two formulas can be written as

$$\tilde{K} = 4.6\times10^{-9}[b_T R_{\rm HB}(1+\tilde{U})]^{0.70} \quad \text{and} \tag{9}$$

$$\tilde{K} = 2.0\times10^{-9}[R_{\rm HM}(1+\tilde{U})]^{0.69}. \tag{10}$$

The fit coefficients, especially the power law exponents, of two equations are close due to the similarity in the formulation of

Brought to you by IFREMER/BIBLIOTHEQUE LA | Unauthenticated | Downloaded 10/10/22 09:59 AM UTC

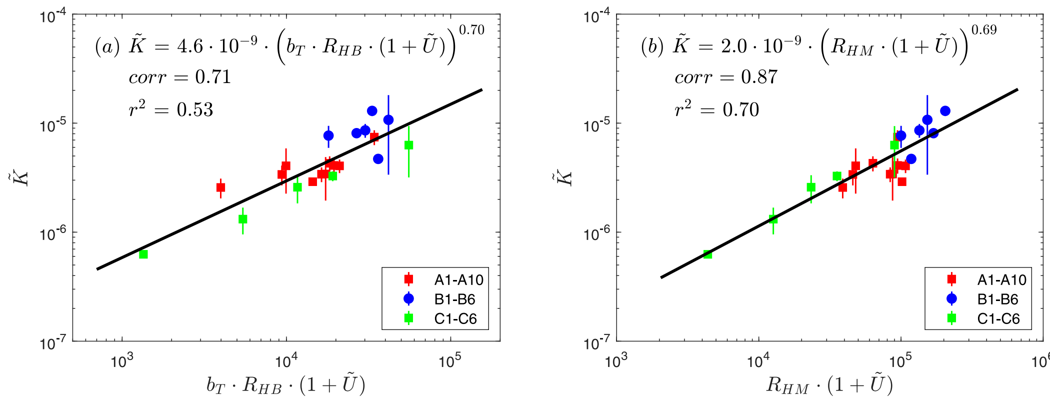

FIG. 9. The parameterization of CO_2 gas transfer, with the computed correlation coefficient and r^2. The $\tilde{K}$ is a main function of wave parameters $b_T R_{HB}$ or R_{HM}. The wind effect is secondary and is expressed as $(1 + \tilde{U})$. The error bars of $\tilde{K}$ represent the standard error of the mean.

R_{HB} and R_{HM}. We reserve the two equations since they stress the influences of waves on gas transfer from different aspects. Both equations could be used for the prediction of gas transfer velocity, although Eq. (10) seems preferable with regard to the correlation coefficient and r^2 value. However, b_T in Eq. (9) could curb the estimation of gas fluxes in regional area (e.g., the tropics) where breaking rate is low.

4. Discussion and conclusions

Equations (9) and (10) highlight the importance of waves in facilitating gas transfer through the main function R_{HB} and R_{HM}. The variable R_{HB} or R_{HM} can be interpreted as a Reynolds number, which is a measure of the turbulence intensity induced by waves. Not only are the similar Reynolds numbers [e.g., R_H and R_B in Eq. (2)] proposed for the study of gas transfer (Woolf 2005; Toba et al. 2006; Brumer et al. 2017), but also the concept of R_{HM} is applied for the research of upper-ocean mixed layer depth, which is affected by wave-induced turbulence (Babanin 2006). Parameters R_{HB} and R_{HM} contain wave height and orbital velocity as the representative scales of length and speed, respectively. The wave orbital velocity is used also because water mass moves along with wave orbital motion, which is related to the surface renewal model for gas exchange studied by Komori et al. (1993).

The wind force in the experiments transfers energy into the waves and creates turbulence beyond water surface. Thus, the wind truly influences gas exchange and the wind speed is found well correlated with gas transfer velocity within each experimental series of B1–B6 or C1–C6 in Figs. 5i and 5k. The critical issue is to parameterize the wind effect. The wind-based formula may be disadvantaged with regard to different wave states as discussed earlier. For the Reynolds number R_H and R_B in Eq. (2), wind friction velocity and a wave parameter (e.g., H_s) are equally weighted. But it is actually the wave that dominates CO_2 gas transfer. In addition, R_H and R_B cannot be used for no-wind conditions when there are still breaking waves (nonlinear interaction of waves) or swells. Although swell is not included in our experiments, it could promote the mixing in water surface layer (Dai et al. 2010). Brumer et al. (2017) also mentioned the importance of swells for gas exchange. In this study, we scale the wind as $(1 + \tilde{U})$, which is compatible for no-wind conditions (experiments A1–A10) and denotes the secondary role of the wind. The results in Fig. 8 show that the correlation is improved after combining $(1 + \tilde{U})$ with wave function $b_T R_{HB}$ or R_{HM}. It should be mentioned that R_H is also well correlated with $\tilde{K}$ based on the results of experiments B1–B6 and C1–C6 as in Fig. 10a. Our Eq. (10) in Fig. 10b produces similar distribution while Eq. (9) in Fig. 10c yields a relatively low correlation. With limited number of points from experimental series B and C, it is difficult to determine which formula is better. More data are needed to compare the parameterizations.

The breaking waves are responsible for both production of excessive amount of turbulence (Agrawal et al. 1992) and bubbles. The turbulence that is related with energy loss during wave breaking could be determined by both breaking probability and breaking strength. In Fig. 5a, there is only weak correlation between gas transfer rate and breaking probability b_T for cases A1–A10. In Fig. 6a, the gas transfer rate is in positive correlation with b_T within each series of experiments, but the results of all cases cannot be reconciled by b_T only. The energy loss of breaking waves cannot be precisely computed in our experiments through Eq. (5). The measurement of H_{b1} and H_{b2} should be conducted at the position of incipient breakers and residual waves after breaking, which varies during experiments. The wave gauges in our experiments are fixed. The wave height measured by gauge 4 may also be subject to modulation after breaking. So we cautiously assume that the drop of wave height between gauge 3 and 4 (e.g., waves marked with a star in Fig. 3) is mainly caused by the loss of energy during breaking while there are other influencing factors. Bubbles can be visually observed in our experiments. However, the dependence of gas transfer on bubbles is not explicitly parameterized in the equations. No consensus has been reached on bubble behavior and size distribution affected by breaking waves. The whitecap coverage, which is empirically described by wind speed, can be employed to denote bubble plume. Some studies prefer the physically based method by correlating bubble injection rate (m s^{-1}) with energy dissipation rate (W m^{-2}) of breaking waves (Fairall et al. 2011; Long et al. 2011).

Brought to you by IFREMER/BIBLIOTHEQUE LA | Unauthenticated | Downloaded 10/10/22 09:59 AM UTC

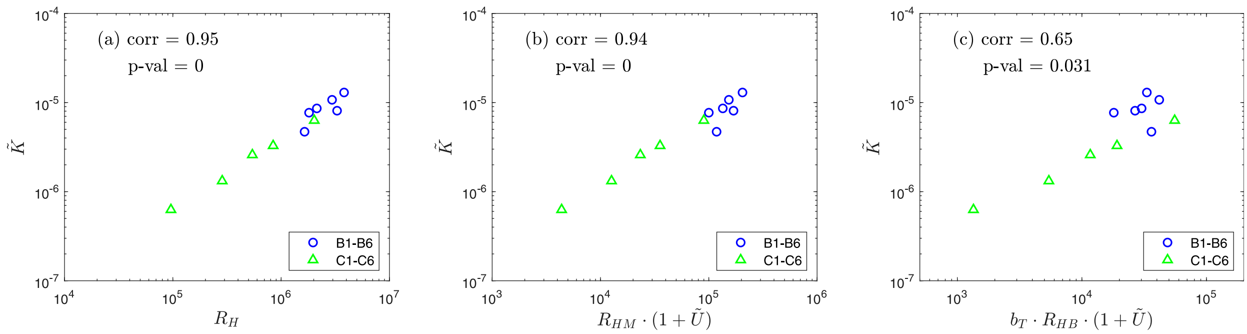

FIG. 10. The nondimensional gas transfer velocity of experiments B1–B6 and C1–C6 vs (a) R_H in Eq. (2), (b) $R_{HM}(1 + \tilde{U})$ in Eq. (10), and (c) $b_T R_{HB}(1 + \tilde{U})$ in Eq. (9).

The Reynolds number R_{HB} or R_{HM} in this study is a measure of wave-induced turbulence, so they could possibly also be related to bubble injection rate, although further evidence is needed.

Last, we summarize the main findings in this work. The wave parameters including wave height and orbital velocity are found well correlated with the gas transfer velocity. New Reynolds numbers R_{HB} and R_{HM} are formulated based on the analysis of experimental results. The gas transfer velocity is further parameterized with a main function of waves and a secondary factor of scaled wind speed.

Acknowledgments. Author Li was supported by the DISI Australia-China Centre through Grant ACSRF48199. Author Babanin acknowledges support from the U.S. Office of Naval Research Grant N00014-17-1-3021. Authors Li and Babanin acknowledge U.S. ONR Global support through Grant N62909-20-1-2080. Author Qiao was jointly supported by the National Natural Science Foundation of China under grants 41821004 and the international cooperation project of the China-Australia Research Centre for Maritime Engineering of Ministry of Science and Technology, China under grant 2016YFE0101400. The authors thank Dr. Ming Xin and Mr. Chao Li for valuable assistance in the experiments. The authors are grateful to Dr. Qingxiang Liu for his help in article revision. The authors report no conflict of interest.

Data availability statement. The data that support the findings of this study can be accessed online (https://doi.org/10.17632/rh6n3npp4d.1).

REFERENCES

Agrawal, Y., E. Terray, M. Donelan, P. Hwang, A. Williams, W. M. Drennan, K. Kahma, and S. Krtaigorodskii, 1992: Enhanced dissipation of kinetic energy beneath surface waves. *Nature*, **359**, 219–220, https://doi.org/10.1038/359219a0.

Asher, W., L. Karle, B. Higgins, P. Farley, E. Monahan, and I. Leifer, 1996: The influence of bubble plumes on air-seawater gas transfer velocities. *J. Geophys. Res.*, **101**, 12 027–12 041, https://doi.org/10.1029/96JC00121.

Babanin, A. V., 2011: *Breaking and Dissipation of Ocean Surface Waves*. Cambridge University Press, 480 pp.

——, 2006: On a wave-induced turbulence and a wave-mixed upper ocean layer. *Geophys. Res. Lett.*, **33**, L20605, https://doi.org/10.1029/2006GL027308.

——, D. Chalikov, I. Young, and I. Savelyev, 2007: Predicting the breaking onset of surface water waves. *Geophys. Res. Lett.*, **34**, L07605, https://doi.org/10.1029/2006GL029135.

——, ——, ——, and ——, 2010: Numerical and laboratory investigation of breaking of steep two-dimensional waves in deep water. *J. Fluid Mech.*, **644**, 433–463, https://doi.org/10.1017/S002211200999245X.

——, T. Waseda, T. Kinoshita, and A. Toffoli, 2011: Wave breaking in directional fields. *J. Phys. Oceanogr.*, **41**, 145–156, https://doi.org/10.1175/2010JPO4455.1.

Bakker, D. C., and Coauthors, 2016: A multi-decade record of high-quality fCO_2 data in version 3 of the surface ocean CO_2 Atlas (SOCAT). *Earth Syst. Sci. Data*, **8**, 383–413, https://doi.org/10.5194/essd-8-383-2016.

Ballantyne, A., C. Alden, J. Miller, P. Tans, and J. White, 2012: Increase in observed net carbon dioxide uptake by land and oceans during the past 50 years. *Nature*, **488**, 70–72, https://doi.org/10.1038/nature11299.

Bell, T. G., and Coauthors, 2017: Estimation of bubble-mediated air–sea gas exchange from concurrent DMS and CO_2 transfer velocities at intermediate–high wind speeds. *Atmos. Chem. Phys.*, **17**, 9019–9033, https://doi.org/10.5194/acp-17-9019-2017.

Benjamin, T. B., and J. Feir, 1967: The disintegration of wave trains on deep water. *J. Fluid Mech.*, **27**, 417–430, https://doi.org/10.1017/S002211206700045X.

Brumer, S. E., C. J. Zappa, B. W. Blomquist, C. W. Fairall, A. Cifuentes-Lorenzen, J. B. Edson, I. M. Brooks, and B. J. Huebert, 2017: Wave-related Reynolds number parameterizations of CO_2 and DMS transfer velocities. *Geophys. Res. Lett.*, **44**, 9865–9875, https://doi.org/10.1002/2017GL074979.

Dai, D., F. Qiao, W. Sulisz, L. Han, and A. Babanin, 2010: An experiment on the nonbreaking surface-wave-induced vertical mixing. *J. Phys. Oceanogr.*, **40**, 2180–2188, https://doi.org/10.1175/2010JPO4378.1.

Delire, C., and Coauthors, 2019: The global land carbon cycle simulated with ISBA-CTRIP: Improvements over the last decade. *J. Adv. Model. Earth Syst.*, **12**, e2019MS001886, https://doi.org/10.1029/2019MS001886.

Denvil-Sommer, A., M. Gehlen, M. Vrac, and C. Mejia, 2019: LSCE-FFNN-v1: A two-step neural network model for the reconstruction of surface ocean pCO2 over the global ocean. *Geosci. Model Dev.*, **12**, 2091–2105, https://doi.org/10.5194/gmd-12-2091-2019.

DeVries, T., and Coauthors, 2019: Decadal trends in the ocean carbon sink. *Proc. Natl. Acad. Sci. USA*, **116**, 11 646–11 651, https://doi.org/10.1073/pnas.1900371116.

Brought to you by IFREMER/BIBLIOTHEQUE LA | Unauthenticated | Downloaded 10/10/22 09:59 AM UTC

Edson, J., and Coauthors, 2011: Direct covariance measurement of CO_2 gas transfer velocity during the 2008 southern ocean gas exchange experiment: Wind speed dependency. *J. Geophys. Res.*, **116**, C00F10, https://doi.org/10.1029/2011JC007022.

Fairall, C., and Coauthors, 2011: Implementation of the coupled ocean-atmosphere response experiment flux algorithm with CO_2, dimethyl sulfide, and O_3. *J. Geophys. Res.*, **116**, C00F09, https://doi.org/10.1029/2010JC006884.

Frew, N. M., and Coauthors, 2004: Air-sea gas transfer: Its dependence on wind stress, small-scale roughness, and surface films. *J. Geophys. Res.*, **109**, C08S17, https://doi.org/10.1029/2003JC002131.

Friedlingstein, P., and Coauthors, 2019: Global carbon budget 2019. *Earth Syst. Sci. Data*, **11**, 1783–1838, https://doi.org/10.5194/essd-11-1783-2019.

Galchenko, A., A. V. Babanin, D. Chalikov, I. Young, and B. K. Haus, 2012: Influence of wind forcing on modulation and breaking of one-dimensional deep-water wave groups. *J. Phys. Oceanogr.*, **42**, 928–939, https://doi.org/10.1175/JPO-D-11-083.1.

Gemmrich, J., 2010: Strong turbulence in the wave crest region. *J. Phys. Oceanogr.*, **40**, 583–595, https://doi.org/10.1175/2009JPO4179.1.

Ho, D. T., C. S. Law, M. J. Smith, P. Schlosser, M. Harvey, and P. Hill, 2006: Measurements of air-sea gas exchange at high wind speeds in the southern ocean: Implications for global parameterizations. *Geophys. Res. Lett.*, **33**, L16611, https://doi.org/10.1029/2006GL026817.

IPCC, 2014: *Climate Change 2014: Synthesis Report*. IPCC, 151 pp., http://www.ipcc.ch/report/ar5/syr/.

Ishidoya, S., S. Aoki, D. Goto, T. Nakazawa, S. Taguchi, and P. Patra, 2012: Time and space variations of the O_2/N_2 ratio in the troposphere over Japan and estimation of the global CO_2 budget for the period 2000–2010. *Tellus*, **64B**, 18964, https://doi.org/10.3402/tellusb.v64i0.18964.

Iwano, K., N. Takagaki, R. Kurose, and S. Komori, 2013: Mass transfer velocity across the breaking air–water interface at extremely high wind speeds. *Tellus*, **65B**, 21341, https://doi.org/10.3402/tellusb.v65i0.21341.

Jähne, B., K. Münnich, and U. Siegenthaler, 1979: Measurements of gas exchange and momentum transfer in a circular wind-water tunnel. *Tellus*, **31**, 321–329, https://doi.org/10.3402/tellusa.v31i4.10440.

——, K. O. Münnich, R. Bösinger, A. Dutzi, W. Huber, and P. Libner, 1987: On the parameters influencing air-water gas exchange. *J. Geophys. Res.*, **92**, 1937–1949, https://doi.org/10.1029/JC092iC02p01937.

Jones, S. D., C. Le Quéré, C. Rödenbeck, A. C. Manning, and A. Olsen, 2015: A statistical gap-filling method to interpolate global monthly surface ocean carbon dioxide data. *J. Adv. Model. Earth Syst.*, **7**, 1554–1575, https://doi.org/10.1002/2014MS000416.

Komori, S., R. Nagaosa, and Y. Murakami, 1993: Turbulence structure and mass transfer across a sheared air–water interface in wind-driven turbulence. *J. Fluid Mech.*, **249**, 161–183, https://doi.org/10.1017/S0022112093001120.

Krall, K. E., A. W. Smith, N. Takagaki, and B. Jähne, 2019: Air–sea gas exchange at wind speeds up to $85\,m\,s^{-1}$. *Ocean Sci.*, **15**, 1783–1799, https://doi.org/10.5194/os-15-1783-2019.

Landschützer, P., N. Gruber, and D. C. Bakker, 2016: Decadal variations and trends of the global ocean carbon sink. *Global Biogeochem. Cycles*, **30**, 1396–1417, https://doi.org/10.1002/2015GB005359.

——, ——, ——, and U. Schuster, 2014: Recent variability of the global ocean carbon sink. *Global Biogeochem. Cycles*, **28**, 927–949, https://doi.org/10.1002/2014GB004853.

Lee, J., J. Monty, J. Elsnab, A. Toffoli, A. Babanin, and A. Alberello, 2017: Estimation of kinetic energy dissipation from breaking waves in the wave crest region. *J. Phys. Oceanogr.*, **47**, 1145–1150, https://doi.org/10.1175/JPO-D-16-0273.1.

Lenain, L., and W. K. Melville, 2017: Measurements of the directional spectrum across the equilibrium saturation ranges of wind-generated surface waves. *J. Phys. Oceanogr.*, **47**, 2123–2138, https://doi.org/10.1175/JPO-D-17-0017.1.

Liang, J.-H., C. Deutsch, J. C. McWilliams, B. Baschek, P. P. Sullivan, and D. Chiba, 2013: Parameterizing bubble-mediated air-sea gas exchange and its effect on ocean ventilation. *Global Biogeochem. Cycles*, **27**, 894–905, https://doi.org/10.1002/gbc.20080.

Liss, P. S., and L. Merlivat, 1986: Air-sea gas exchange rates: Introduction and synthesis. *The Role of Air-Sea Exchange in Geochemical Cycling*, P. Buat-Ménard, Ed., Springer, 113–127.

Long, M. S., W. C. Keene, D. Kieber, D. Erickson, and H. Maring, 2011: A sea-state based source function for size- and composition-resolved marine aerosol production. *Atmos. Chem. Phys.*, **11**, 1203–1216, https://doi.org/10.5194/acp-11-1203-2011.

McGillis, W. R., and Coauthors, 2004: Air-sea CO_2 exchange in the equatorial Pacific. *J. Geophys. Res.*, **109**, C08S02, https://doi.org/10.1029/2003JC002256.

Melville, W. K., 1996: The role of surface-wave breaking in air-sea interaction. *Annu. Rev. Fluid Mech.*, **28**, 279–321, https://doi.org/10.1146/annurev.fl.28.010196.001431.

Nightingale, P. D., G. Malin, C. S. Law, A. J. Watson, P. S. Liss, M. I. Liddicoat, J. Boutin, and R. C. Upstill-Goddard, 2000: In situ evaluation of air-sea gas exchange parameterizations using novel conservative and volatile tracers. *Global Biogeochem. Cycles*, **14**, 373–387, https://doi.org/10.1029/1999GB900091.

Ocampo-Torres, F., M. Donelan, N. Merzi, and F. Jia, 1994: Laboratory measurements of mass transfer of carbon dioxide and water vapour for smooth and rough flow conditions. *Tellus*, **46B**, 16–32, https://doi.org/10.3402/tellusb.v46i1.15746.

Rödenbeck, C., R. F. Keeling, D. C. Bakker, N. Metzl, A. Olsen, C. Sabine, and M. Heimann, 2013: Global surface-ocean pCO_2 and sea–air CO_2 flux variability from an observation-driven ocean mixed-layer scheme. *Ocean Sci.*, **9**, 193–216, https://doi.org/10.5194/os-9-193-2013.

Stanley, R. H., W. J. Jenkins, D. E. Lott III, and S. C. Doney, 2009: Noble gas constraints on air-sea gas exchange and bubble fluxes. *J. Geophys. Res.*, **114**, C11020, https://doi.org/10.1029/2009JC005396.

Sutherland, P., and W. K. Melville, 2015: Field measurements of surface and near-surface turbulence in the presence of breaking waves. *J. Phys. Oceanogr.*, **45**, 943–965, https://doi.org/10.1175/JPO-D-14-0133.1.

Sweeney, C., E. Gloor, A. R. Jacobson, R. M. Key, G. McKinley, J. L. Sarmiento, and R. Wanninkhof, 2007: Constraining global air-sea gas exchange for CO_2 with recent bomb ^{14}C measurements. *Global Biogeochem. Cycles*, **21**, GB2015, https://doi.org/10.1029/2006GB002784.

Takahashi, T., and Coauthors, 2009: Climatological mean and decadal change in surface ocean pCO_2, and net sea–air CO_2 flux over the global oceans. *Deep-Sea Res. II*, **56**, 554–577, https://doi.org/10.1016/j.dsr2.2008.12.009.

——, S. C. Sutherland, and A. Kozyr, 2019: Global ocean surface water partial pressure of CO_2 database: Measurements performed during 1957–2018 (version 2018). NOAA/NCEI/OCADS

Brought to you by IFREMER/BIBLIOTHEQUE LA | Unauthenticated | Downloaded 10/10/22 09:59 AM UTC

NDP-088(V2018) Rep., 25 pp., https://www.ncei.noaa.gov/access/ocean-carbon-data-system/oceans/LDEO_Underway_Database/NDP-088_V2018.pdf.

Thomson, J., M. S. Schwendeman, S. F. Zippel, S. Moghimi, J. Gemmrich, and W. E. Rogers, 2016: Wave-breaking turbulence in the ocean surface layer. *J. Phys. Oceanogr.*, **46**, 1857–1870, https://doi.org/10.1175/JPO-D-15-0130.1.

Toba, Y., S. Komori, Y. Suzuki, and D. Zhao, 2006: Similarity and dissimilarity in air-sea momentum and CO_2 transfers: The nondimensional transfer coefficients in light of windsea Reynolds number. *Atmosphere–Ocean Interactions*, Vol. 2, W. Perrie, Ed., WIT Press, 53–82.

Tulin, M. P., and T. Waseda, 1999: Laboratory observations of wave group evolution, including breaking effects. *J. Fluid Mech.*, **378**, 197–232, https://doi.org/10.1017/S0022112098003255.

Wanninkhof, R., 1992: Relationship between wind speed and gas exchange over the ocean. *J. Geophys. Res.*, **97**, 7373–7382, https://doi.org/10.1029/92JC00188.

——, W. E. Asher, D. T. Ho, C. Sweeney, and W. R. McGillis, 2009: Advances in quantifying air-sea gas exchange and environmental forcing. *Annu. Rev. Mar. Sci.*, **1**, 213–244, https://doi.org/10.1146/annurev.marine.010908.163742.

——, and Coauthors, 2013: Global ocean carbon uptake: Magnitude, variability and trends. *Biogeosciences*, **10**, 1983–2000, https://doi.org/10.5194/bg-10-1983-2013.

Waseda, T., and M. P. Tulin, 1999: Experimental study of the stability of deep-water wave trains including wind effects. *J. Fluid Mech.*, **401**, 55–84, https://doi.org/10.1017/S0022112099006527.

Woolf, D. K., 2005: Parametrization of gas transfer velocities and sea-state-dependent wave breaking. *Tellus*, **57B**, 87–94, https://doi.org/10.3402/tellusb.v57i2.16783.

——, and Coauthors, 2007: Modelling of bubble-mediated gas transfer: Fundamental principles and a laboratory test. *J. Mar. Syst.*, **66**, 71–91, https://doi.org/10.1016/j.jmarsys.2006.02.011.

Zappa, C. J., W. Asher, and A. Jessup, 2001: Microscale wave breaking and air-water gas transfer. *J. Geophys. Res.*, **106**, 9385–9391, https://doi.org/10.1029/2000JC000262.

——, ——, ——, J. Klinke, and S. Long, 2004: Microbreaking and the enhancement of air-water transfer velocity. *J. Geophys. Res.*, **109**, C08S16, https://doi.org/10.1029/2003JC001897.

Zhao, D., and Y. Toba, 2001: Dependence of whitecap coverage on wind and wind-wave properties. *J. Oceanogr.*, **57**, 603–616, https://doi.org/10.1023/A:1021215904955.

——, ——, Y. Suzuki, and S. Komori, 2003: Effect of wind waves on air–sea gas exchange: Proposal of an overall CO_2 transfer velocity formula as a function of breaking-wave parameter. *Tellus*, **55B**, 478–487, https://doi.org/10.1034/j.1600-0889.2003.00055.x.

Brought to you by IFREMER/BIBLIOTHEQUE LA | Unauthenticated | Downloaded 10/10/22 09:59 AM UTC